Genetically encoded calcium indicator illuminates calcium dynamics in primary cilia

Steven Su[1–3,8], Siew Cheng Phua[2,3,8], Robert DeRose[2,3], Shuhei Chiba[4], Keishi Narita[5], Peter N Kalugin[2,3], Toshiaki Katada[6], Kenji Kontani[6], Sen Takeda[5] & Takanari Inoue[2,3,7]

Visualization of signal transduction in live primary cilia constitutes a technical challenge owing to the organelle's submicrometer dimensions and close proximity to the cell body. Using a genetically encoded calcium indicator targeted to primary cilia, we visualized calcium signaling in cilia of mouse fibroblasts and kidney cells upon chemical or mechanical stimulation with high specificity, high sensitivity and wide dynamic range.

The vertebrate primary cilium is a solitary hair-like structure that protrudes from the plasma membrane into the extracellular space, and functions as a sensory organelle for detecting diverse chemical[1–3] and mechanical[4,5] stimuli. Each cilium measures 0.2 µm in diameter and a few micrometers in length, and takes up only 1/10,000th of the total cell volume. Visualization of ciliary signal transduction evoked by extracellular stimuli is difficult because of the organelle's submicrometer size as well as researchers' inability to dissect cilia-specific signals from the activity in the main cell body. Emerging evidence supports the role of calcium ions (Ca^{2+}) as a principal secondary messenger of ciliary signaling pathways. Ca^{2+}-permeable channels of the transient receptor potential (TRP) channel family localize to primary cilia, and Ca^{2+} fluxes through these ion channels have been proposed to have major roles in signal transduction induced by mechanical and thermal stimuli as well as G protein–coupled receptor signaling[6–9]. An electrophysiological method to measure signals in primary cilia has been previously reported[10], but the submicrometer size of this organelle makes patch-clamping the ciliary membrane difficult. Synthetic Ca^{2+} indicator dyes allow the monitoring of multiple cells but often result in signal saturation of the entire cytosol that overwhelms local transient Ca^{2+} fluxes in specific subcellular compartments (**Supplementary Fig. 1**).

Here we report a strategy to specifically target genetically encoded Ca^{2+} indicators (GECIs) into primary cilia to distinguish cilia-specific Ca^{2+} signaling from that of the main cell body. We first evaluated a collection of ciliary targeting sequences (CTSs)[11], which included two truncated peptides derived from the cytoplasmic tail of fibrocystin (CTS20 and CTS68), full-length 5-hydroxytryptamine (serotonin) receptor isoform 6 ($5HT_6$), a fusion peptide consisting of the transmembrane domain of integrin β1 and the C-terminal domain of Arl13b (integrin-Arl13b; IA) as well as a $5HT_6$-CTS20 combination. We tagged each CTS with GFP and evaluated these constructs for targeting efficiencies and effects on cilia morphology (**Supplementary Figs. 2** and **3**). $5HT_6$-GFP and IA-GFP demonstrated high cilia-targeting efficiencies of 87% (131/150 GFP-expressing cells) and 85% (146/172 GFP-expressing cells), respectively (**Supplementary Figs. 2a** and **3e**,**g**). None of the CTSs tested had an obvious effect on ciliation frequency, indicating that overexpression of CTSs in cells did not adversely affect ciliogenesis (**Supplementary Fig. 2b**). Expression of $5HT_6$-GFP and IA-GFP, however, caused the average length of primary cilia to increase approximately twofold, (**Supplementary Fig. 2c**) and correlated with a higher frequency of morphological deformations (**Supplementary Figs. 2d** and **4**).

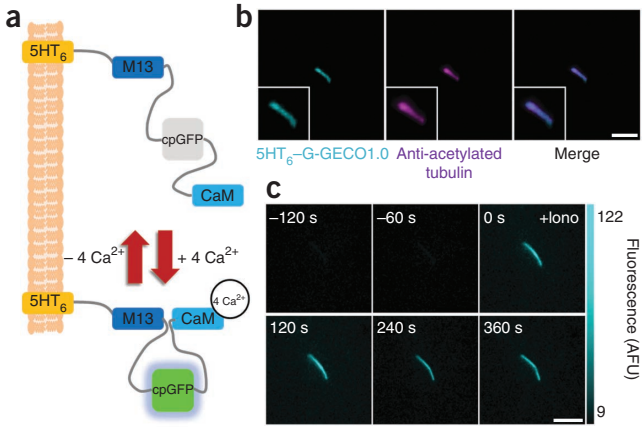

Figure 1 | $5HT_6$–G-GECO1.0 targets primary cilia and detects changes in ciliary Ca^{2+}. (**a**) Schematic of $5HT_6$–G-GECO1.0, containing M13 (a skeletal muscle light-chain kinase), a circularly permuted GFP (cpGFP) and calmodulin (CaM). (**b**) A primary cilium from a NIH-3T3 cell expressing $5HT_6$–G-GECO1.0 stained with antibody against acetylated α-tubulin. Scale bar, 3 µm. Insets show magnified cilia. (**c**) Time-lapse imaging of a NIH-3T3 primary cilium expressing $5HT_6$–G-GECO1.0 at indicated times relative to addition of ionomycin (+Iono). AFU, arbitrary fluorescence unit. Scale bar, 5 µm.

[1]Department of Biomedical Engineering, Whiting School of Engineering, Johns Hopkins University, Baltimore, Maryland, USA. [2]Department of Cell Biology, School of Medicine, Johns Hopkins University, Baltimore, Maryland, USA. [3]Center for Cell Dynamics, School of Medicine, Johns Hopkins University, Baltimore, Maryland, USA. [4]Graduate School of Life Sciences, Tohoku University, Sendai, Miyagi, Japan. [5]Department of Anatomy and Cell Biology, Interdisciplinary Graduate School of Medicine and Engineering, University of Yamanashi, Yamanashi, Japan. [6]Department of Physiological Chemistry, Graduate School of Pharmaceutical Sciences, University of Tokyo, Tokyo, Japan. [7]Precursory Research for Embryonic Science and Technology, Japan Science and Technology Agency, Saitama, Japan. [8]These authors contributed equally to this work. Correspondence should be addressed to T.I. (jctinoue@jhmi.edu).

RECEIVED 24 APRIL; ACCEPTED 13 AUGUST; PUBLISHED ONLINE 22 SEPTEMBER 2013; DOI:10.1038/NMETH.2647

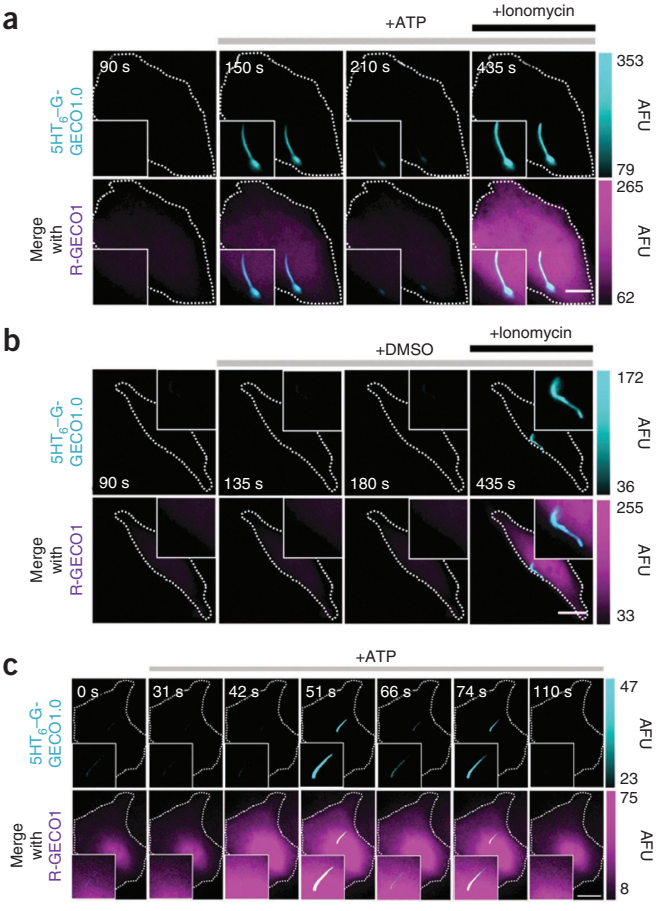

Figure 2 | $5HT_6$–G-GECO1.0 detects ciliary Ca^{2+} influxes in response to ATP. (**a**,**b**) Fluorescence microscopy images of NIH-3T3 cells expressing the indicated sensors, showing response to ATP (**a**) or DMSO (**b**). Scale bars, 5 µm. Time-lapse imaging was initiated at 0 s, and images were captured at 0.067 Hz. (**c**) High-speed time lapse imaging (0.63 Hz) reveals oscillations in cytosolic and ciliary Ca^{2+} in response to 10 µM ATP in NIH-3T3 cells expressing indicated sensors. Scale bar, 10 µm. AFU, arbitrary fluorescence unit. Dotted lines indicate cell boundaries.

Nevertheless, the bulk of primary cilia expressing these two constructs exhibited regular morphology. Transmission electron microscopy and immunofluorescence studies of $5HT_6$-expressing primary cilia demonstrated no obvious defects in cilia ultrastructure as well as normal localization of key ciliary proteins (**Supplementary Figs. 5** and **6**).

We next fused these CTSs with currently available GECIs, including intramolecular CFP and YFP fluorescence resonance energy transfer (FRET) indicators TNXXL[12] and YC3.60 (ref. 13), as well as single fluorescence GFP indicators G-CaMP5G[14] and G-GECO1.0 (ref. 15) (**Supplementary Table 1**). We characterized the cilia-targeting efficiency and signal dynamic range of each CTS-tagged GECI (**Supplementary Figs. 7–9**). $5HT_6$–G-GECO1.0 (**Fig. 1a**) demonstrated the greatest potential as a cilia-specific Ca^{2+} indicator and was comparable with $5HT_6$-GFP in cilia-targeting efficiency, ciliation efficiency and effects on ciliary structure (**Fig. 1b** and **Supplementary Figs. 2–4**). At the basal state, $5HT_6$–G-GECO1.0 displayed weak GFP fluorescence in primary cilia but exhibited an increase of 360.0% ± 62.1% (± s.e.m., $n = 13$ cells) in GFP fluorescence when stimulated with 2 µM ionomycin (**Fig. 1c**, **Supplementary Fig. 9a**, **Supplementary Table 1** and **Supplementary Video 1**). All subsequent experiments were conducted with $5HT_6$–G-GECO1.0.

ATP triggers increases in cellular calcium levels via the activation of ATP-gated P2X calcium-permeable channels and/or G protein–coupled P2Y receptors, which induce the mobilization of intracellular Ca^{2+} from inositol 1,4,5-trisphosphate-sensitive stores. We therefore investigated whether ciliary Ca^{2+} changes could be detected in response to ATP stimulation. Through the co-expression of cytosolic R-GECO1 (a single red fluorescent GECI)[15] and cilia-targeted $5HT_6$–G-GECO1.0 in NIH-3T3 cells, we detected a pronounced rise in cytosolic Ca^{2+} that was accompanied by a comparable increase in ciliary Ca^{2+} in 52.2% (12/23) of cells stimulated by 10 µM ATP (**Fig. 2a**). We observed an average maximum increase of 53.9% ± 20.4% (± s.e.m., $n = 11$ cells) and 54.3% ± 10.0% (± s.e.m., $n = 11$ cells) in fluorescence intensity in the cilia and the cytosol, respectively (**Supplementary Fig. 10a**). In contrast, vehicle control did not generate any Ca^{2+} response in the cytosol and primary cilia (**Fig. 2b** and **Supplementary Fig. 10b**). To determine the source of observed ciliary Ca^{2+} fluxes, we increased our imaging frequency from 0.067 Hz to 0.63 Hz. We observed that spikes in cytosolic Ca^{2+} clearly preceded ciliary Ca^{2+} spikes in 100% (14/14) of cells (**Fig. 2c**, **Supplementary Fig. 10c** and **Supplementary Video 2**). The average delay time between the cytosolic and ciliary Ca^{2+} elevation was 6.04 s ± 0.98 s (± s.e.m.; $n = 14$ cells). Consistent with this, whenever we detected Ca^{2+} oscillations in the cytosol, we also observed correlated but delayed calcium spikes in the cilia. (**Fig. 2c**, **Supplementary Fig. 10c** and **Supplementary Video 2**). Furthermore, ciliary Ca^{2+} fluxes propagated in a base-to-tip direction in the ciliary lumen in 100% (14/14) of ATP-induced ciliary Ca^{2+} spikes detected (**Supplementary Fig. 11** and

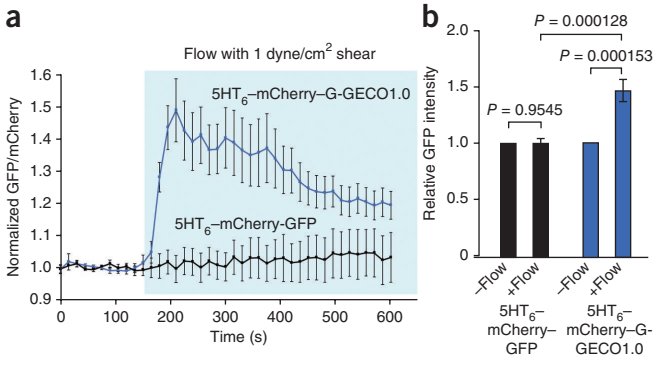

Figure 3 | Laminar fluid flow induces dynamic calcium signals in primary cilia. (**a**) Fluorescence intensity of GFP divided by that of mCherry before and after (light blue box) administration of flow. $5HT_6$–mCherry–G-GECO1.0 activity was measured for 18 primary cilia from 7 independent experiments and $5HT_6$–mCherry–GFP (control) activity was measured in 9 primary cilia from 3 independent experiments. Fluorescence signals were normalized against baseline fluorescence before induction of flow. Error bars, s.e.m. ($n = 18$ for $5HT_6$–m-Cherry-G-GECO1.0 and $n = 9$ for $5HT_6$–mCherry-GFP). (**b**) Comparison of relative GFP intensities between $5HT_6$–mCherry–G-GECO1.0 and $5HT_6$–mCherry–GFP before and after 1 min of flow induction. Error bars, s.e.m. ($n = 18$ for $5HT_6$–mCherry-G-GECO1.0 and $n = 9$ for $5HT_6$–mCherry-GFP).

Supplementary Video 3). Collectively, these observations suggest that the ciliary Ca^{2+} flux originates from the calcium stores in the cytosol. However, we cannot exclude other possibilities such as a contribution of ATP-gated P2X calcium-permeable channels localized at the base of primary cilia. By further increasing the imaging frequency to 1.5 Hz, we calculated the linear rate of Ca^{2+} propagation along the ciliary shaft to be 0.83 ± 0.22 μm/s (± s.d.) in cilia where the Ca^{2+} propagated the entire length of the lumen ($n = 11$ cells). Of note, these numbers could be at least partially affected by buffering effect from overexpressed $5HT_6$–G-GECO1.0. Because GFP-based GECIs are sensitive to changes in pH[16], we confirmed that ciliary pH did not change with ATP by using a newly developed ciliary pH biosensor, $5HT_6$-CFP-Venus(H148G) (**Supplementary Fig. 12**).

Finally, we asked whether we could detect Ca^{2+} dynamics in primary cilia when subjecting them to a mechanical stimulus. Fluid flow across the apical cell membrane induces bending of the cilia, and the resultant shear force is commonly believed to activate cilia-localized Ca^{2+}-permeable TRPP2 channels[7]. However, the critical step involving the entry of extracellular Ca^{2+} into the ciliary lumen has not been demonstrated. Therefore, we set up a fluid flow system to subject ciliated mouse inner medullary collecting duct (mIMCD3) cells with defined laminar flow. To normalize for the anticipated flow-induced movements of cilia, we transiently expressed $5HT_6$-mCherry-G-GECO1.0 in cells such that cilia spatial movements could be visualized by the mCherry fluorescence marker (**Supplementary Fig. 13a**,**b**). Initiation of fluid flow (with wall shear stress corresponding to a physiological value of 1 dyne/cm^2) induced the immediate bending of cilia (**Supplementary Fig. 13c** and **Supplementary Video 4**), whereas specific bending behavior of each primary cilium was dependent on parameters such as spatial orientation and cilium length. Flow initiation also induced a pronounced increase in ciliary Ca^{2+} which initiated within 15 s of flow induction on average, and attained peak responses at 1 min after induction of flow (**Fig. 3a**, **Supplementary Fig. 13c** and **Supplementary Video 4**). To validate that the observed changes in GFP fluorescence in primary cilia were indicative of genuine changes in GECI activity and were not due to ciliary movement, we ascertained that flow initiation did not induce a significant change in GFP fluorescence in cilia expressing $5HT_6$-mCherry-GFP ($P = 0.9545$), whereas cilia expressing $5HT_6$–mCherry–G-GECO1.0 exhibited an average 1.46-fold increase in GFP fluorescence 1 min after induction of flow (**Fig. 3** and **Supplementary Fig. 14**). Additional work is required to elucidate the source of Ca^{2+} signaling observed.

The intermediate affinity of G-GECO1.0 for Ca^{2+} (K_d value of 749 nM)[15] is of sufficient sensitivity to detect changes in Ca^{2+} concentrations in primary cilia when cells are stimulated with ATP and mechanical flow. Nevertheless, other forms of signaling stimuli may induce lower concentration ranges of ciliary Ca^{2+} that may not be detectable by G-GECO1.0. For these applications, it may be necessary to target GECIs with lower K_d values to the primary cilia. The successful application of the cilia-targeted GECI also serves as a proof of concept to extend this approach to visualize other signaling molecules in primary cilia.

METHODS

Methods and any associated references are available in the online version of the paper.

Accession codes. GenBank, European Molecular Biology Laboratory and DNA Data Bank of Japan: NM_021358 ($5HT_6$), NM_153179.2 (fibrocystin), NM_001174150 (Arl13b) and NM_002211 (β1 integrin receptor).

Note: Any Supplementary Information and Source Data files are available in the online version of the paper.

ACKNOWLEDGMENTS

We thank A. Seki and T. Meyer (Stanford University) for the $5HT_6$ construct, M. Fivaz (National University of Singapore) for the Lyn-YFP construct, A. Miyawaki (RIKEN) for the YC3.60 construct, L. Looger (Janelia Farm) for the GCaMP5G construct, G. Pazour (University of Massachusetts) for the GFP-CTS20 and GFP-CTS68 constructs, O. Griesbeck (Max Planck Institute) for the TNXXL construct, R. Reed (Johns Hopkins University) for mIMCD3 cells, and Y. Okubo, K. Kanemaru and H. Ishikawa for helpful comments on the manuscript. This study was supported in part by the US National Institutes of Health (NIH) (GM092930, DK065655 and DK090868 pilot funds provided by the Baltimore Polycystic Kidney Disease Research and Clinical Core Center) to T.I., and other grants to S.C., K.N., S.T., K.K. and T.K. from the Ministry of Education, Culture, Sports, Science and Technology of Japan and the Japan Society for the Promotion of Science. S.C.P. is supported by the Agency for Science, Technology and Research in Singapore.

AUTHOR CONTRIBUTIONS

S.S., S.C.P., R.D., P.N.K. and T.I. generated constructs. K.K. developed the IA sequence under the supervision of T.K. The immunohistochemistry was performed by S.C., and K.N. and S.T. took the transmission electron microscopy images. S.S., S.C.P., R.D. and P.N.K. carried out cell biology experiments and microscopy under the supervision of T.I. S.C.P., S.S. and T.I. wrote the manuscript.

COMPETING FINANCIAL INTERESTS

The authors declare no competing financial interests.

1. Christensen, S., Clement, C., Satir, P. & Pedersen, L. *J. Pathol.* **226**, 172–184 (2012).
2. Singla, V. & Reiter, J.F. *Science* **313**, 629–633 (2006).
3. Berbari, N., Johnson, A., Lewis, J., Askwith, C. & Mykytyn, K. *Mol. Biol. Cell* **19**, 1540–1547 (2008).
4. Praetorius, H.A. & Spring, K.R. *J. Membr. Biol* **184**, 71–79 (2001).
5. Whitfield, J.F. *Cell. Signal.* **20**, 1019–1024 (2008).
6. Köttgen, M. *et al. J. Cell Biol.* **182**, 437–447 (2008).
7. Nauli, S.M. *et al. Nat. Genet.* **33**, 129–137 (2003).
8. Belgacem, Y.H. & Borodinsky, L.N. *Proc. Natl. Acad. Sci. USA* **108**, 4482–4487 (2011).
9. Bai, C.-X. *et al. EMBO Rep.* **9**, 472–479 (2008).
10. Kleene, N. & Kleene, S. *Cilia* **1**, 17 (2012).
11. Nachury, M.V., Seeley, E.S. & Jin, H. *Annu. Rev. Cell Dev. Biol.* **26**, 59–87 (2010).
12. Mank, M. *et al. Nat. Methods* **5**, 805–811 (2008).
13. Horikawa, K. *et al. Nat. Methods* **7**, 729–732 (2010).
14. Akerboom, J. *et al. J. Neurosci.* **32**, 13819–13840 (2012).
15. Zhao, Y. *et al. Science* **333**, 1888–1891 (2011).
16. Mank, M. & Griesbeck, O. *Chem. Rev.* **108**, 1550–1564 (2008).

ONLINE METHODS

DNA construct availability. All DNA plasmids are available through Addgene.

Construction of the β1Int-HaloTag-Arl13b–C-GFP (IA-GFP) expression vector. DNA encoding the human Arl13b C-terminal region (amino acids 355–428 of Arl13b)[17] was amplified using PCR primers (5′-cccaagcttaggaaccaccgggtagaacc and 5′-aggtc gactgagatcacatcatgagcatca) and subcloned into pEGFP-C-CMV5 (a modified pCMV5 mammalian expression vector encoding C-terminal GFP-fusion protein). DNA encoding β1Int-HaloTag[18] was then subcloned into pEGFP-C-CMV5/Arl13b(355–428) to make the β1Int-HaloTag-Arl13b–C-GFP expression vector.

Construction of the Lyn-GFP expression vector. *GFP* was subcloned into sequence encoding Lyn-YFP (Clontech pYFP-N1 vector; gift from M. Fivaz) using AgeI and BsrGI to replace *YFP*.

Construction of the $5HT_6$-GFP-CTS20 expression vector. DNA encoding $5HT_6$ flanked by AgeI was amplified by PCR primers (5′-ctactgaccggtcgccaccatggttccagagcccggccctgtcaacag and 5′-gct gacaccggtcctcctgcgctaccaccagcactgttcatgggggaaccaagtgg) from sequence encoding $5HT_6$-GFP[19] (Clontech pEGFP-N3 vector; gift from A. Seki and T. Meyer), and then subcloned into the 5′ AgeI site of sequence encoding GFP-CTS20 (ref. 20) (Clontech pEGFP-C2 vector; gift from G. Pazour). *CTS20* sequence encodes residues 1–20 of the N-terminal cytoplasmic tail of fibrocystin.

Construction of the $5HT_6$-YC3.60 expression vector. DNA encoding $5HT_6$ flanked by HindIII was amplified by PCR primers (5′-catccgaagcttgccaccatggttccagagc and 5′-gcacctaagctttcctcct gcgcttcctcctgcgctctttgagattcgtcggaacacatgataatag) from sequence encoding $5HT_6$-GFP[19] (Clontech pEGFP-N3 vector) and then subcloned into a YC3.60 vector (gift from A. Miyawaki).

Construction of the $5HT_6$-G-GECO1.0 expression vector. DNA encoding $5HT_6$ flanked by BamHI was amplified by PCR primers (5′-cattcaggatccgccaccatggttccagagc and 5′-gcatctggatcctcctcc tgcgctaccacca) from sequence encoding $5HT_6$-GFP[19] (Clontech pEGFP-N3 vector) and then subcloned into CMV-G-GECO1.0 vector (obtained from Addgene).

Construction of the $5HT_6$-G-CaMP expression vector. DNA encoding G-CaMP5G (gift from L. Looger) flanked with BamHI and HindIII was amplified by PCR primers (5′-ctactggga tccagtgctggtggtagcgcaggaggaatgggttctcatcatcatcatcatcatgg and 5′-gcaacatagttaagaataccagtcaatctttcac) and then subcloned into a $5HT_6$-CFP-FKBP vector[21] in replacement of *CFP-FKBP*.

Construction of the TNXXL-CTS20 expression vector. First, the stop codon was removed from the 3′ end of the TNXXL sequence (gift from O. Griesbeck) by site-directed mutagenesis (Stratagene) using PCR primers (5′-cgaggactacgaattctgcagatatccatcacactggc ggcc and 5′-ggccgccagtgtgatggatatctgcagaattcgtagtcctcg). The resulting vector was digested with EcoRI and ligated to *CTS20* digested with EcoRI from a GFP-CTS20 vector.

Construction of the TNXXL-CTS68 expression vector. The TNXXL vector with no stop codon was digested with EcoRI and then ligated to *CTS68* digested with EcoRI from a GFP-CTS20 vector. *CTS68* encodes residues 1–68 of the N-terminal cytoplasmic tail of fibrocystin.

Construction of the $5HT_6$–mCherry–G-GECO1.0. DNA encoding G-GECO1.0 was digested from CMV-G-GECO1.0 vector using BamHI and EcoRI and subcloned into a sequence encoding $5HT_6$-mCherry (pmCherry-C1, Clontech) that had been digested with BglII and EcoRI.

Construction of the $5HT_6$-mCherry-GFP expression vector. *GFP* was digested from sequence encoding $5HT_6$-GFP (pEGFP-N3, Clontech) using Acc65I and BsrGI and subcloned into a sequence encoding $5HT_6$-mCherry (pmCherry-C1, Clontech) that had been digested with Acc65I.

Construction of the $5HT_6$-CFP-Venus(H148G) expression vector. Sequence encoding $5HT_6$-CFP was first constructed by subcloning sequence encoding $5HT_6$ into a CFP vector using NheI and AgeI. Sequence encoding Venus(H148G) flanked with EcoRI and BamHI was then amplified by PCR primers (5′-catccggaat tcgatggtgagcaagggcgagg and 5′-gcagtgggatccttacttgtacagctcgt ccatgcc) and subcloned into the $5HT_6$-CFP vector.

Cell culture and transfection. NIH-3T3 cells and mIMCD3 cells containing an integrated *FRT* site in the genome (gift from R. Reed) were cultured in DMEM (Gibco) supplemented with 10% FBS. For all transient transfections, cells were transfected with the respective DNA constructs by plating them directly in a transfection solution containing DNA plasmid and FuGENE HD (Roche). Cells were plated on poly(D-lysine)-coated borosilicate glass Lab-Tek 8-well chambers (Thermo Scientific). Ciliogenesis was induced by serum starvation for 24 h. For flow experiments, transfected cells were seeded into Microslide VI$^{0.4}$ channels (ibidi) at a cell suspension density of approximately 1.3×10^6 cells/ml to achieve confluence.

Immunofluorescence. To mark primary cilia, NIH-3T3 cells were fixed with 4% (w/v) paraformaldehyde, permeabilized with 0.1% (v/v) Triton X-100 and immunostained with mouse monoclonal anti–acetylated tubulin antibody (Sigma, T7451, 1:2,000 dilution) and secondary anti-mouse antibody conjugated to Alexa Fluor 568 (Invitrogen, 1:1,000 dilution). For immunostaining of IMCD3 cells, cells were grown on cover slips, transfected with vector encoding 5HT6-YFP, cultured for 72 h, washed with phosphate-buffered saline (PBS) and fixed with ice-cold methanol at −20 °C for 7 min. Fluorescence images were obtained using a LSM710 confocal microscope (Carl Zeiss) equipped with a Plan Apochromat ×100 oil-immersion objective lens (NA 1.4) and processed using ImageJ software. The antibodies used include rabbit polyclonal antibodies against pericentrin (Babco, PRB-432C, 1:250 dilution), NPHP3 (Proteintech, 22026-1-AP, 1:1,000 dilution), IFT88 (Proteintech, 13967-1-AP, 1:750 dilution), Arl13b (Proteintech, 17711-1-AP, 1:1,000 dilution), Cep164 (Novus, 45330002, 1:4,000 dilution), Cep290 (Bethyl Laboratories, A301-659A, 1:1,000 dilution), and mouse monoclonal antibodies against acetylated α-tubulin (Sigma; 6-11B-1, T7451, 1:1000 dilution), γ-tubulin (Sigma; GTU-88, T-6557, 1:1000 dilution) and poly(Glu-tubulin) (Enzo; GT335, ALX-804-885-C100, 1:1,000

doi:10.1038/nmeth.2647

dilution). The secondary antibodies used in this study were Alexa Fluor 568–labeled anti-mouse IgG (Molecular Probes, 1:1,500 dilution) and Alexa Fluor 633–labeled anti-rabbit IgG (Molecular Probes, 1:2,000 dilution).

Transmission electron microscopy. For the ultrastructural analysis of cilia overexpressing $5HT_6$-GFP or GFP alone, the genes encoding these proteins were introduced into NIH-3T3 cells using a lentiviral expression system developed by H. Miyoshi at the RIKEN BioResource Center[22]. For the expression of $5HT_6$-GFP, the cDNA was amplified with KOD DNA polymerase and ligated into the Eco47III site of CSII-CMV-MCS-IRES2-Bsd. For the expression of GFP alone, the CS-CDF-CG-PRE was used. These expression constructs were packaged into infectious viral particles[22] and added to the NIH-3T3 culture medium at the multiplicity of infection of >20. After the viral transduction, cells expressing $5HT_6$-GFP were selected with 30 μM blasticidin. Expression of $5HT_6$-GFP or GFP alone in most if not all cells was confirmed by fluorescence microscopy. Preparations of the cells and observation of cilia by transmission electron microscopy were carried out principally according to the previous study[23] with slight modifications. Briefly, cultured cells were fixed with a half Karnovsky's solution (2% paraformaldehyde and 2.5% glutaraldehyde in 0.1 M cacodylate buffer, pH 7.5) supplemented with 1% tannic acid for 30 min at room temperature, followed by rinse with 10% sucrose in cacodylate buffer (pH 7.5) three times. The cells were post-fixed with 1% osmium tetroxide for 30 min on ice, followed by extensive irrigation with ice-cold distilled water. Subsequently, the cells were stained en bloc with 1% uranyl acetate in 50% ethanol for 2 h, dehydrated with a series of graded concentration of ethanol and embedded in epoxy resin. The cells in the epoxy block were cut by the LKB2088 ultramicrotome (Stockholm), mounted onto formvar-reinforced single slot grids, and stained with uranyl acetate and lead citrate. The samples were observed under the Hitachi H-7500 transmission electron microscope (Tokyo). Images of ciliary cross-sections were analyzed with ImageJ to measure the ciliary diameter.

Epi-fluorescence imaging. Most of the imaging experiments were performed on an Axiovert135TV epi-fluorescence microscope (Zeiss) with 63× oil objective (Zeiss), and images were collected by a QIClick charge-coupled device (CCD) camera (QImaging). For the dual-color epi-fluorescence imaging under flow conditions, IX-71 (Olympus) microscope was used together with a 40× oil objective (Olympus) and a CoolSNAP HQ CCD camera (Photometrics). Imaging was driven by Metamorph 7.5 imaging software (Molecular Devices). All calcium imaging experiments were performed in Dulbecco's Phosphate-Buffered Saline (Gibco) containing 0.9 mM [Ca^{2+}], except for the characterization of the cytosolic dynamic range of each CTS-GECI, which was performed in DMEM with 25 mM HEPES (Gibco). All pH imaging experiments were performed in DMEM with 25 mM HEPES (Gibco). All imaging experiments were completed at room temperature (21–23 °C). FRET images were thresholded to remove background before any contrast adjustments.

Ciliary and cytoplasmic pH determination. NIH-3T3 cells were transfected with either vector encoding $5HT_6$-CFP-Venus(H148G) for cilia measurements, or vector encoding CFP plus vector encoding Venus(H148G) for cytoplasmic measurements. For measurements of fluorescence ratios at known pH, cells were washed once with DMEM plus HEPES at the chosen pH, then allowed to sit in DMEM plus HEPES at the known pH containing 5 μM each of the H^+ ionophores nigericin and monensin (both Sigma) for 5 min to equilibrate. Approximately 8–10 cilia were analyzed at each chosen pH point. All fluorescence ratios are normalized to an initial measurement at pH 7.4. For determination of pH in cilia and cytoplasm, cells were placed in DMEM plus HEPES at the standard pH of 7.4 with no H^+ ionophores and imaged.

Flow system coupled with epi-fluorescence time-lapse imaging. Syringe pump (Model 230, KD Scientific) was used to provide unidirectional laminar flow when connected with cell-seeded microchannel slides. DPBS (Gibco) was used as flow perfusate. Using the Poiseuille equation for rectangular channels, $\tau = 6\mu Q/bh^2$ (where τ is shear stress, μ is medium viscosity, Q is the flow rate, b is channel width and h is channel height), a flow rate of 0.6 ml/min was provided by the syringe pump to provide a shear stress of approximately 1 dyne/cm^2 within the microchannel. In these experiments, only upright-positioned cilia were imaged. Each cilium was imaged at 0.067 Hz for 2 min before flow was initiated for a period of ~7.5 min. Imaging was continued for an additional 4 min after flow was stopped. At each time point, each primary cilium was imaged in the *x-y* plane with nine *z*-stacks (separated by 1 μm). A total of 18 cells from seven independent experiments were imaged and quantified for $5HT_6$–mCherry–G-GECO1.0, and a total of nine cells from three independent experiments were imaged and quantified for $5HT_6$-mCherry-GFP. Notably, the flow-induced calcium response was found to be sensitive to environmental changes. Each imaging experiment was performed at room temperature (21–23 °C), and was completed within 1 h after cells were taken out from an incubator 37 °C. Fluorescence images shown in **Supplementary Figure 13c** and **Supplementary Video 4** are *z*-projections of nine consecutive *x-y* planes. GFP and corresponding mCherry cilia images have been normalized against background signal variation. GFP divided by mCherry fluorescence ratio cilia images were obtained by taking the fluorescence ratio of background-normalized GFP and background-normalized mCherry signal intensities and represented in pseudocolor scale. These values have been further subjected to two other steps of normalization, (i) normalization against signal area variation and (ii) normalization against basal signal intensities (before flow), and presented in graph plots in **Figure 3a** as normalized measurements of GFP divided by mCherry fluorescence ratios in response to flow stimulation.

17. Hori, Y. *et al. Biochem. Biophys. Res. Commun.* **373**, 119–124 (2008).
18. Svendsen, S. *et al. BMC Cell Biol.* **9**, 17 (2008).
19. Berbari, N.F. *et al. Mol. Biol. Cell* **19**, 1540–1547 (2008).
20. Follit, J.A. *et al. J. Cell Biol.* **188**, 21–28 (2010).
21. Lin, Y.C. *et al. Nat. Chem. Biol.* **9**, 437–443 (2013).
22. Honda, A. *et al. J. Biol. Chem.* **285**, 31362–31369 (2010).
23. Narita, K. *et al. Traffic* **11**, 287–301 (2010).